E-cadherin and LGN align epithelial cell divisions with tissue tension independently of cell shape

Kevin C. Hart[a], Jiongyi Tan[b], Kathleen A. Siemers[a], Joo Yong Sim[c], Beth L. Pruitt[c,d,e,f], W. James Nelson[a,d], and Martijn Gloerich[a,1,2]

[a]Department of Biology, Stanford University, Stanford, CA 94305; [b]Biophysics Program, Stanford University, Stanford, CA 94305; [c]Department of Mechanical Engineering, Stanford University, Stanford, CA 94305; [d]Department of Molecular and Cellular Physiology, Stanford University, Stanford, CA 94305; [e]Department of Bioengineering, Stanford University, Stanford, CA 94305; and [f]Cardiovascular Institute, Stanford University, Stanford, CA 94305

Edited by Masatoshi Takeichi, RIKEN Center for Developmental Biology, Kobe, Japan, and approved June 6, 2017 (received for review February 9, 2017)

Tissue morphogenesis requires the coordinated regulation of cellular behavior, which includes the orientation of cell division that defines the position of daughter cells in the tissue. Cell division orientation is instructed by biochemical and mechanical signals from the local tissue environment, but how those signals control mitotic spindle orientation is not fully understood. Here, we tested how mechanical tension across an epithelial monolayer is sensed to orient cell divisions. Tension across Madin–Darby canine kidney cell monolayers was increased by a low level of uniaxial stretch, which oriented cell divisions with the stretch axis irrespective of the orientation of the cell long axis. We demonstrate that stretch-induced division orientation required mechanotransduction through E-cadherin cell–cell adhesions. Increased tension on the E-cadherin complex promoted the junctional recruitment of the protein LGN, a core component of the spindle orientation machinery that binds the cytosolic tail of E-cadherin. Consequently, uniaxial stretch triggered a polarized cortical distribution of LGN. Selective disruption of *trans* engagement of E-cadherin in an otherwise cohesive cell monolayer, or loss of LGN expression, resulted in randomly oriented cell divisions in the presence of uniaxial stretch. Our findings indicate that E-cadherin plays a key role in sensing polarized tensile forces across the tissue and transducing this information to the spindle orientation machinery to align cell divisions.

cell–cell adhesion | cell division orientation | mitotic spindle | mechanotransduction

Epithelial tissues undergo dramatic morphological changes during development to acquire their correct 3D organization (1). Morphogenesis requires the coordinated regulation of cell division orientation, because the subsequent position of daughter cells within the tissue affects cell fate and epithelial architecture (2). In simple epithelia, planar cell divisions maintain a single-layered tissue architecture, and the angle of division within this plane determines the direction of epithelial expansion and consequently tissue shape (3). In contrast, cell divisions along the apico–basal axis induce multilayering, which underlies cell differentiation in stratified epithelia such as the epidermis (4), and may contribute to loss of epithelial organization in tumors (5).

The plane of cell division is specified by the position of the mitotic spindle, which in mammalian tissues is defined by the cortical distribution of the protein LGN (6, 7). This evolutionarily conserved adaptor protein orients the mitotic spindle by providing cortical anchorage sites for astral microtubules of the spindle and applying a pulling force on those microtubules through the associated proteins NuMA and dynein (7). Recently, we showed that LGN is recruited to E-cadherin–based cell–cell contacts during interphase (8). E-cadherin couples neighboring cells to each other through homotypic interactions of its extracellular domain, and associates with the actin cytoskeleton through catenin proteins bound to its cytosolic tail (9). LGN adopts a 3D structure similar to the cadherin-bound catenins, and is recruited to cell–cell junctions by direct binding to the cytosolic tail of E-cadherin to ensure epithelial cells divide within the plane of the epithelium (8).

Epithelial morphogenesis is directed by instructive signals received by cells from their microenvironment, including local activation of signaling receptors by biochemical cues (1). In addition, cells are subject to diverse mechanical forces, including tensile forces exerted by neighboring cells and by contraction of the intracellular actomyosin cytoskeleton (10, 11). These mechanical forces are sensed by cells and transduced into an intracellular response, which triggers changes in cellular behaviors, including cell proliferation, differentiation, and migration (12, 13). Cells possess different mechanisms to sense mechanical forces across tissues, which includes a major role for E-cadherin (10, 14). Tension on E-cadherin junctions, generated by forces exerted on its extracellular domain or cytosolic tail, induces an adaptive reinforcement of cell–cell adhesion (15), which involves changes in the molecular organization of the E-cadherin–catenin complex and its association with the actin cytoskeleton (16–18). Mechanotransduction through E-cadherin further triggers intracellular signaling events including activation of transcriptional programs (19).

During zebrafish epiboly (20) and growth of the *Drosophila* wing imaginal disk (21, 22), planar cell divisions are aligned with the direction of tissue tension. This alignment of cell divisions has been attributed to the shape of cells, because cells were

Significance

Tissue morphogenesis requires coordinated regulation of cellular behavior through instructive signals from the local tissue environment, including mechanical forces exerted by neighboring cells. The cell–cell adhesion protein E-cadherin plays an important role in converting tensile forces across the tissue into an intracellular response to regulate actin cytoskeleton organization, reinforce cell–cell adhesion, and activate transcriptional programs. We show E-cadherin also transduces these forces to orient the mitotic spindle, which occurs irrespectively of tension-induced changes in cell shape and instead involves regulation of junctional recruitment of the protein LGN, a core component of the spindle orientation machinery. Because the orientation of cell division controls tissue architecture, these findings support a key role of E-cadherin in mechanical regulation of tissue morphogenesis.

Author contributions: K.C.H., J.Y.S., B.L.P., W.J.N., and M.G. designed research; K.C.H., K.A.S., and M.G. performed research; J.T. and J.Y.S. contributed new reagents/analytic tools; K.C.H., J.T., K.A.S., J.Y.S., and M.G. analyzed data; and K.C.H., W.J.N., and M.G. wrote the paper.

The authors declare no conflict of interest.

This article is a PNAS Direct Submission.

Freely available online through the PNAS open access option.

[1]Present address: Molecular Cancer Research, Center for Molecular Medicine, University Medical Center, Utrecht 3584CG, The Netherlands.

[2]To whom correspondence should be addressed. Email: m.gloerich@umcutrecht.nl.

This article contains supporting information online at www.pnas.org/lookup/suppl/doi:10.1073/pnas.1701703114/-/DCSupplemental.

elongated along the main axis of tension, and the mitotic spindle typically orients along the long axis of the cell in the absence of other instructive cues (23). This conclusion is supported by a strong correlation between the orientation of the long axis of cells and the direction of cell division upon stretching suspended epithelial monolayers in vitro (24). However, other mechanisms that may transduce tensile forces across epithelial monolayers to the mitotic spindle might contribute to cell division orientation along the axis of tension. Because E-cadherin has a prominent role in mechanosensing and orienting cell divisions, we hypothesized that E-cadherin may couple tensile forces across a tissue to the orientation of the mitotic spindle.

Here, we increased tension across a Madin–Darby canine kidney (MDCK) cell monolayer with a low level of uniaxial stretch that minimized effects on cell elongation. Significantly, we showed that cell divisions aligned with the stretch axis, irrespective of the orientation of the cell long axis. Instead, stretch-induced orientation of epithelial divisions required *trans* engagement of E-cadherin and involved tension-dependent recruitment of LGN to cell–cell adhesions. Our results provide evidence that mechanosensing by E-cadherin adhesions transduces tensile forces across the tissue through LGN to the mitotic spindle to align epithelial cell divisions.

Results

Previously, it was shown that high levels of stretch (30%) of suspended epithelial cell monolayers induced both cell elongation and division orientation in the direction of stretch (24). We sought to test whether lower, more physiological levels of uniaxial stretch (25) also affected division orientation. We fabricated a simple stretch device compatible with live-cell imaging and the application of low levels of uniaxial stretch to a cell monolayer adhering to an extracellular matrix (ECM) substrate. This device is composed of a stretchable silicone membrane, optically suitable for fluorescence imaging, bonded to the bottom of microfabricated polydimethylsiloxane (PDMS) silicone channels (Fig. 1*A*). The central channel membrane was coated with collagen I and seeded with MDCK cells, which recapitulate the organization and function of a simple, single-layered epithelial tissue. The cell monolayer was stretched by applying vacuum pressure to the two neighboring side channels using a pneumatic controller, which resulted in uniaxial outward deflection of the sidewalls surrounding the central channel (Fig. 1*A*). Measurement of the displacement of fluorescent microspheres dispersed on the silicone membrane showed that there was a monotonic increase of strain with increasing vacuum pressure up to ∼15% strain in the direction of applied stretch (ε_{xx}), with negligible levels of strain perpendicular to this direction (ε_{yy}) or shear strain (ε_{xy}) (Fig. 1*B*). Quantification of the nearest neighbor distance of nuclei in MDCK cell monolayers showed similar levels of strain with increasing vacuum pressure (Fig. 1*C*). All subsequent experiments used a vacuum pressure (12 inches of Hg) to achieve $\varepsilon_{xx} = 12\%$.

To determine the orientation of cell divisions, MDCK cells expressing GFP-tagged α-tubulin were seeded at confluence on the uniaxial stretch device and monitored by live-cell imaging. In the absence of applied stretch, the distribution of spindle angles

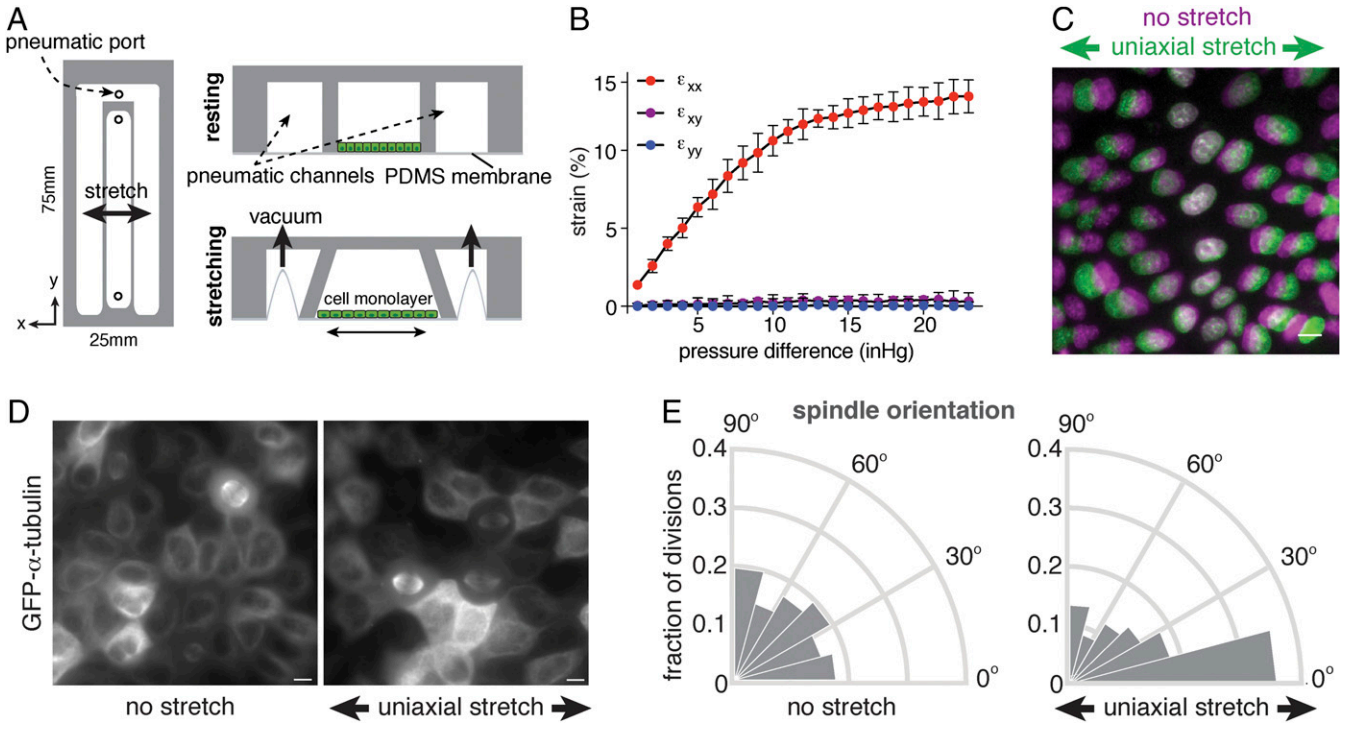

Fig. 1. Epithelial cell divisions align with a low level of uniaxial stretch. (*A*) Design of uniaxial cell stretching device, in which a stretchable silicone membrane is bonded to the bottom of microfabricated PDMS channels. The central channel containing cells is surrounded with pneumatic channels in which vacuum pressure is controlled to induce outward deflection of the channel walls surrounding the cell chamber and stretching of the underlying membrane. (*B*) Substrate strain measured by displacement of microsphere beads in the normal (ε_{yy}), transverse (ε_{xx}), and shear (ε_{xy}) directions, with the mean percentage of strain and SD from three independent experiments. (*C*) Representative example of 12% axial cell strain based on the displacement of nuclei in confluent MDCK monolayers, showing the distribution of nuclei before (magenta) and after (green) application of stretch. (*D*) Visualization of the mitotic spindle in MDCK cells expressing GFP–α-tubulin with and without application of 12% uniaxial stretch (3 h of stretch in this representative image). (*E*) Circular frequency histograms (Rose diagrams) of the mitotic spindle angle relative to the direction of stretch, in MDCK GFP–α-tubulin cells with ($n = 279$) or without ($n = 153$) application of at least 1 h of uniaxial stretch, from three independent experiments. Orientation of cell divisions in the direction of stretch is observed within 1 h of stretch (Fig. S1C). (Scale bars, 10 μm.)

in late metaphase was random (Fig. 1 *D* and *E*). In contrast, 12% axial strain (applied for at least 1 h) induced a strong bias in the orientation of cell divisions in the direction of stretch, with a significant enrichment of cell divisions oriented within 0–15° of the stretch axis (36 ± 6%; compared with 17 ± 2% cells dividing in this direction before application of stretch) (Fig. 1 *D* and *E*; see Fig. S1 *A* and *B* for unbinned data and statistical analyses). Thus, a low level of uniaxial stretch in an epithelial cell monolayer was sufficient to align cell divisions with the stretch axis.

We tested whether cell division orientation in the direction of low level uniaxial stretch correlated with the cell long axis, because division orientation has previously been attributed directly to an effect of anisotropic tension on cell shape (20–22, 24). The long axis of cells relative to the direction of applied stretch was measured in MDCK cell monolayers expressing E-cadherin:DsRed, which marked the boundary of each cell (Fig. 2*A*). Compared with the strong orientation of mitotic spindles with the stretch axis (Fig. 1*E*), we detected only a relatively small increase in the number of interphase cells that were elongated within 0–15° of the stretch axis (20 ± 4%) compared with that in unstretched cells (15 ± 3%) (Fig. 2*B* and Fig. S1*D*). Furthermore, the distribution of aspect ratios of the cell long and short axes was comparable in unstretched and stretched conditions (Fig. S1 *F* and *G*), indicating that 12% uniaxial stretch had little effect on the overall shape of cells in an ECM-attached MDCK cell monolayer.

Next, we directly compared cell division orientation with interphase cell shape. For this, we measured the long axis of cells

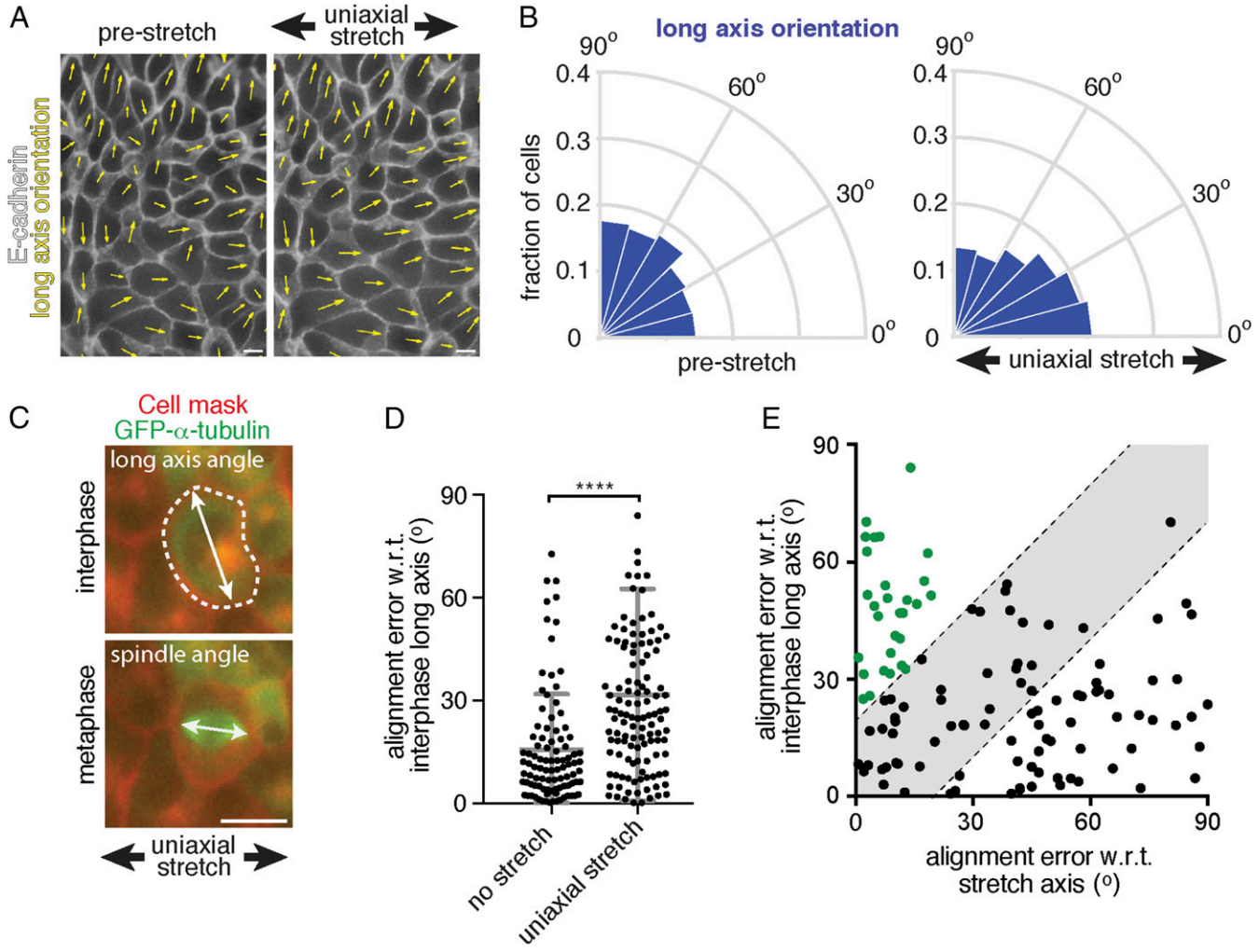

Fig. 2. Alignment of cell divisions with low-level uniaxial stretch does not correspond to interphase cell shape. (*A*) Representative image of the analysis of the angle of the cell long axis, indicated with yellow arrows, in MDCK cells expressing E-cadherin:DsRed (shown in white) before and after the application of 12% uniaxial stretch. (*B*) Circular frequency histograms (Rose diagrams) of the distribution of the long axis angle relative to the direction of stretch in MDCK E-cadherin:DsRed cells before and after uniaxial stretching, from six independent experiments with at least 500 cells per experiment. Images were taken upon 2 min of applied stretch [similar results were obtained with 4 h of applied stretch (Fig. S1*E*)]. (*C*) Example of the measurement of the angle of the cell long axis before entering mitosis, and of the angle of the mitotic spindle in late metaphase, in MDCK cells expressing GFP–α-tubulin in which the plasma membrane is visualized with Cellmask. (*D*) Error in alignment of mitotic spindle orientation with the interphase long axis in cells with a well-defined long axis (aspect ratio >1.4) with and without the application of at least 1 h of 12% uniaxial stretch. Gray bars show the mean alignment error with SD from seven independent experiments; $n = 96$ unstretched and 120 stretched cells. (*E*) Error in alignment of mitotic spindle orientation with the interphase long axis (aspect ratio >1.4) plotted against the error in alignment with the stretch axis in 12% uniaxially stretched monolayers. The gray area indicates divisions that align equally well with the interphase long axis and stretch axis (within 20°). The population of cells that align divisions better with the stretch axis than interphase long axis is indicated in green dots. Data are pooled from seven independent experiments. (Scale bars, 10 μm.) ****$P < 0.0001$. w.r.t., with respect to.

in interphase before mitotic entry, and the angle of the mitotic spindle of the same cells during metaphase (Fig. 2*C*). In the absence of stretch, cells with a well-defined interphase long axis (aspect ratio >1.4) typically divided along their long axis (74 ± 11% of divisions occurred within 15° of the interphase long axis; Fig. 2*D*). Upon application of 12% uniaxial stretch, this correlation between division angle and interphase long axis was strongly reduced (30 ± 12% of division occurred within 15° of the interphase long axis; Fig. 2*D*). By comparing the alignment of cell divisions with the stretch and interphase long axes, we observed a subset of cells in which the division axis was better aligned with the direction of stretch than interphase long axis (Fig. 2*E*, green dots). Moreover, cells dividing in the direction of uniaxial stretch (within 15° of the stretch axis) showed a random distribution of their long axis in interphase (Fig. 2*E* and Fig. S1*H*), compared with cells dividing in that direction before application of stretch (Fig. S1*H*). Thus, a low level of uniaxial stretch caused the orientation of cell divisions in the direction of stretch independently of cell shape. Our analyses also revealed a population of cells in which the division orientation did not appear to respond to stretch and which better aligned with the interphase long axis than the axis of applied stretch (Fig. 2*E*, *Bottom Right* corner), as also observed in suspended cell monolayers under 30% uniaxial stretch (24).

Our results do not exclude a contribution of cell shape in orienting cell divisions under stretch, but they indicate a requirement for additional mechanisms. The cell–cell adhesion protein E-cadherin has a prominent role in orienting cell divisions (8, 26–30) as well as in sensing tensile forces between neighboring cells (31, 32). Tension on E-cadherin junctions can be generated by forces exerted on the extracellular domain by neighboring cells, which can be induced by application of external stretch, and intracellularly through actomyosin contraction (31). Increased tension on the E-cadherin complex triggers an adaptive reinforcement of cell–cell junctions that involves remodeling of the actomyosin cytoskeleton (15, 32–34), including the recruitment of myosin II to cell–cell junctions (35–37). We observed a strong cortical accumulation of GFP-myosin IIA upon application of uniaxial stretch, compared with the diffuse cytoplasmic distribution of GFP-myosin IIA in cells in an unstretched control cell monolayer (Fig. 3 *A* and *B*). Moreover, following uniaxial stretch GFP-myosin IIA displayed a polarized cortical distribution that was enriched at the cell cortex perpendicular to the stretch axis (Fig. 3 *A* and *C*). As these results imply that a low level of axial strain triggers a polarized distribution of tensile forces on E-cadherin junctions, we tested whether mechanosensing by E-cadherin is required to orient cell division under these conditions.

To isolate the role of E-cadherin–mediated cell–cell adhesion in stretch-induced division orientation, we used MDCK cells expressing an N-terminally truncated mutant of E-cadherin (T151) under inducible control of a doxycycline promoter (38). T151 E-cadherin lacks a functional extracellular domain, but has an intact plasma membrane-tethered cytosolic tail that binds catenins and the actin cytoskeleton (38) (Fig. 3*D*). When T151 E-cadherin is expressed, levels of endogenous cadherins are reduced, and thus cells lack intercellular adhesions through E-cadherin (38). However, a cohesive cell monolayer is maintained due to the presence of other cell–cell junctions (38), in contrast to the effects of completely

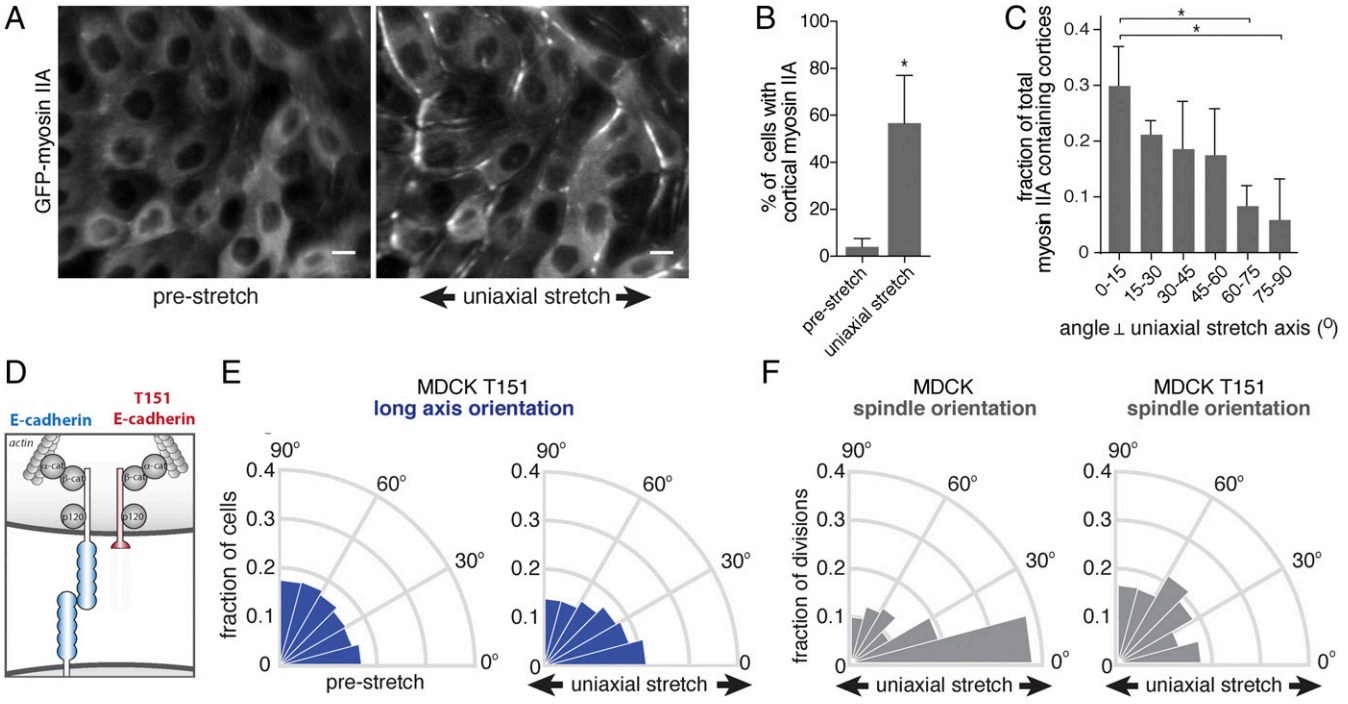

Fig. 3. Uniaxial stretch-oriented division requires E-cadherin adhesion. (*A*) Localization of GFP-myosin IIA in MDCK cells before and after application of 1 h of 12% uniaxial stretch, showing the cortical accumulation of GFP-myosin IIA following uniaxial stretch. (*B*) Quantification of the number of cells with cortical GFP-myosin IIA before and upon application of (at least 1 h of) 12% uniaxial stretch, showing mean with SD of three independent experiments (n = 4,176 unstretched and 3,159 stretched cells). (*C*) Quantification of the distribution of the angle of cortices that contained cortical myosin IIA enrichment upon (at least 1 h of) 12% uniaxial stretch, with mean and SD from three independent experiments (n = 278 cells). (*D*) Schematic representation of the T151 E-cadherin mutant with a truncated extracellular domain. (*E*) Circular frequency histograms (Rose diagrams) of the distribution of the long axis angle relative to the direction of stretch, in MDCK cells expressing T151 E-cadherin, before and after application of 12% stretch, from five independent experiments with at least 500 cells per experiment. (*F*) Circular frequency histograms (Rose diagrams) of the mitotic spindle angle relative to the direction of stretch, with and without application of 12% stretch in parental MDCK (n = 148 cells) and MDCK T151 (n = 285) cells from three independent experiments. (Scale bars, 10 μm.) *P < 0.05.

removing cadherin proteins from MDCK cell monolayers by RNAi depletion, which precludes formation of a cohesive monolayer (26). Due to its truncated extracellular domain, T151 E-cadherin cannot transmit forces between cells, and consequently mechanical stretch cannot exert direct tensile forces on E-cadherin. This enabled us to specifically perturb the role of E-cadherin in stretch-induced epithelial cells that retained cell–cell adhesions.

Similar to control MDCK cells expressing endogenous E-cadherin, uniaxial stretch caused a small redistribution in the angle of the long axis of interphase cells expressing T151 E-cadherin (Fig. 3*E* and Fig. S2*A*). In contrast to control MDCK cells, however, uniaxial stretched cells expressing T151 E-cadherin did not align mitotic spindles with the direction of stretch (Fig. 3*F*; see Fig. S2 *B* and *C* for unbinned data and statistical analyses). Thus, the selective disruption of E-cadherin–mediated cell–cell adhesion was sufficient to inhibit the orientation of cell division with uniaxial stretch, but had little or no effect on stretch-induced orientation of the long axis of those cells. This observation supports our conclusion that uniaxial stretch-induced cell division orientation requires factors other than cell shape, and that E-cadherin cell–cell adhesion is essential to align cell divisions with uniaxial stretch.

Having identified a role of E-cadherin in uniaxial stretch-induced spindle orientation, we investigated whether this role involved LGN, a key component of the spindle orientation machinery. We showed previously that LGN binds the cytosolic tail of E-cadherin to stabilize cortical astral microtubule interactions at E-cadherin adhesions and establish planar epithelial divisions (8). Strikingly, we observed that the junctional recruitment of LGN was dependent on cell density: LGN localized strongly to cell–cell contacts in low-density MDCK monolayers, but was less concentrated at cell–cell junctions and more diffuse in dense monolayers (Fig. 4*A*). At higher monolayer density, MDCK cells become less motile (39) and may consequently exert less tensile forces on each other, and cortical myosin II levels are reduced (Fig. S3). To test whether junctional recruitment of LGN is sensitive to intercellular tensile forces, we increased intercellular tension in high-density cell monolayers uniformly in all directions by applying external biaxial stretch (10%) to monolayers grown on silicone substrates (40). Biaxial stretch resulted in significantly increased levels of LGN at cell–cell contacts, similar to the enrichment of LGN observed at cell–cell contacts in unstretched low-density MDCK cell monolayers (Fig. 4 *A* and *B*). Significantly, this stretch-induced recruitment of LGN was not observed in MDCK cells expressing T151 E-cadherin lacking the extracellular domain (Fig. S4*A*), indicating that this stretch-induced recruitment of LGN requires the transmission of force through the extracellular domain of E-cadherin.

To test further whether tensile forces on E-cadherin regulate the recruitment of LGN to E-cadherin adhesions, we lowered intracellular tensile forces by inhibiting myosin II contraction

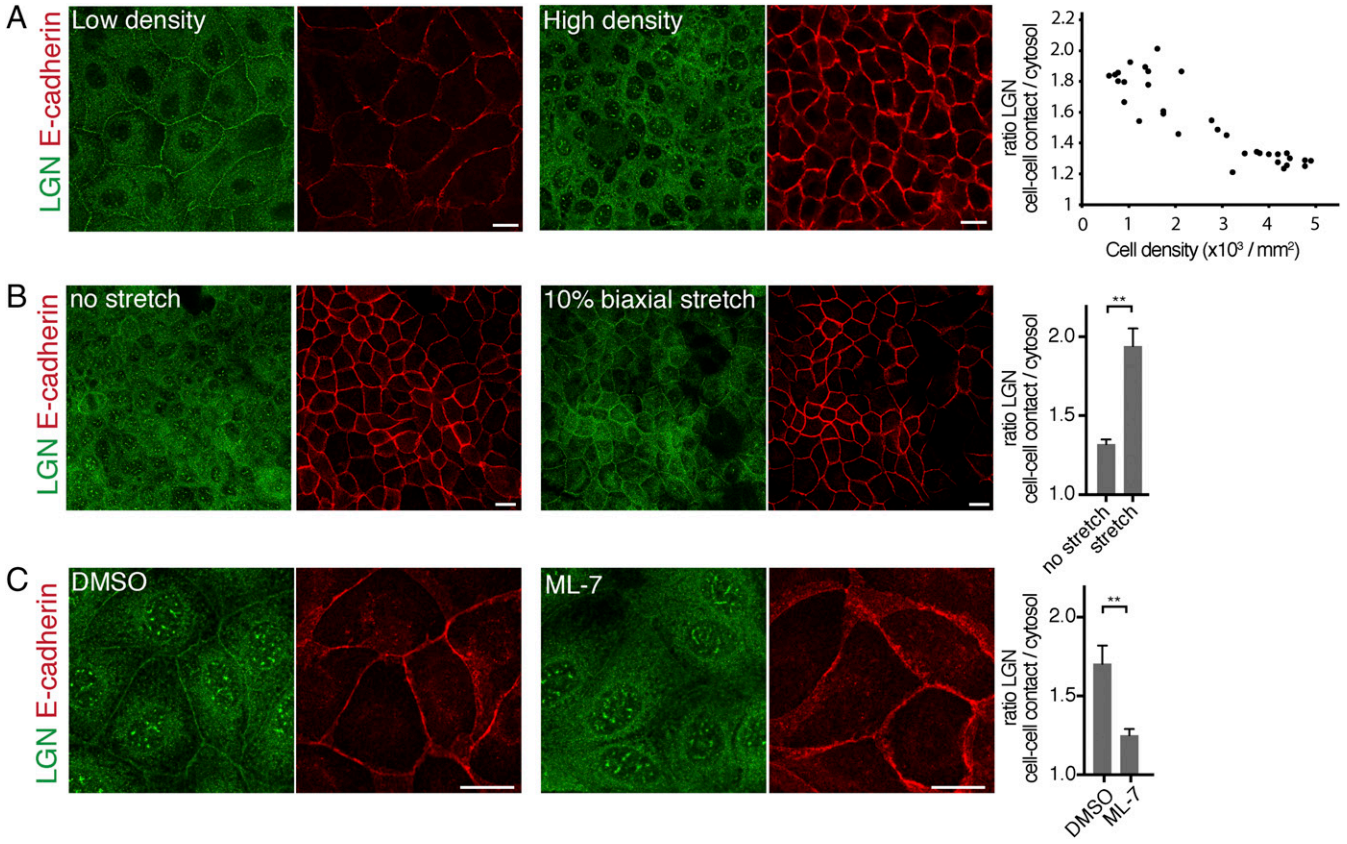

Fig. 4. Recruitment of LGN to the cell cortex is regulated by tension. (*A*) Immunostaining of endogenous LGN and E-cadherin in low-density and high-density MDCK cell monolayers. The quantification shows the ratio of LGN at cell–cell contacts (marked with E-cadherin) versus cytosol in monolayers at different cell densities. Pearson coefficient = −0.893. (*B*) Immunostaining of endogenous LGN and E-cadherin in high-density monolayers MDCK cells upon 10% biaxial stretch. The quantification shows the mean ratio ± SD of LGN at the cell–cell contacts versus cytosol from three independent experiments, with stretch applied for at least 1 h. (*C*) Localization of endogenous LGN and E-cadherin in low-density MDCK monolayers incubated for 5 min with 25 μM ML-7 or vehicle control (DMSO). The quantification shows the mean ratio ± SD of LGN at cell–cell contacts versus cytosol from three independent experiments. (Scale bars, 10 μm.) $^{**}P < 0.005$.

with the selective myosin light chain kinase inhibitor ML-7, which reduces tension on E-cadherin (31). ML-7 treatment resulted in a significant reduction of cortical LGN levels in MDCK cell monolayers grown at low density (Fig. 4 *A* and *C*). To test whether this tension-sensitive cortical recruitment of LGN was due to its recruitment to E-cadherin adhesions specifically, we artificially formed E-cadherin–dependent cell adhesions on microfabricated silicone sidewalls functionalized with the extracellular domain of E-cadherin (41). Single MDCK cells bound to these functionalized sidewalls and LGN was recruited to the E-cadherin complex that formed at the cell–sidewall interface (Fig. S4 *A* and *B*; see also ref. 8). Importantly, LGN recruitment to the cell–sidewall interface was significantly reduced in the presence of ML-7 (Fig. S4 *A*–*C*). Collectively, these results indicate that the recruitment of LGN to E-cadherin–based cell–cell contacts is regulated by tension across the cell monolayer that is sensed by E-cadherin.

Our data imply that the recruitment of LGN to E-cadherin is mechanically regulated, which may underlie the orientation of cell divisions with uniaxial stretch of the cell monolayer. Therefore, we visualized the cellular distribution of LGN in uniaxially stretched cell monolayers. Consistent with a role for LGN in tension-oriented cell divisions, LGN displayed a polarized cortical distribution in interphase cells upon 12% uniaxial stretch (Fig. 5 *A* and *B* and Fig. S5*A*). LGN was enriched at cell–cell contacts perpendicular to the stretch axis (Fig. 5 *A*–*C*), whereas E-cadherin appeared to remain localized uniformly at all cell–cell contacts (Figs. 5*C* and 2*A*). To test directly whether LGN coupled uniaxial stretch of the cell monolayer to cell division orientation, we depleted LGN expression in MDCK cells using shRNAs (Fig. S5*B*). This depletion resulted in the randomization of mitotic spindle alignment with uniaxial stretch (Fig. 5*D* and Fig. S2 *B* and *C*). However, knockdown of LGN expression did not affect the minor redistribution of the long axis angle (Fig. 5*E* and Fig. S2*A*). Altogether, our results show that cell divisions align with uniaxial stretch independently of cell shape, through E-cadherin and LGN.

Discussion

Epithelial development and homeostasis rely on instructive signals from the local environment to coordinate cell behaviors to establish and maintain tissue organization (1). These signals include mechanical forces that are sensed by cells and transduced into intracellular responses (10), which involve a prominent role for the cell–cell adhesion protein E-cadherin. Tension on E-cadherin junctions reinforces cell–cell adhesion (16, 32, 42–44) and triggers intracellular signaling to control gene transcription (12). Here, we demonstrated that E-cadherin transduces tensile forces across a tissue to orient epithelial cell divisions through the tension-sensitive recruitment of LGN, a core component of the spindle orientation machinery.

A role for tissue tension in the orientation of cell division has been demonstrated in vivo during zebrafish epiboly (20) and growth of the *Drosophila* wing imaginal disk (21, 22). In both cases, alignment of divisions was attributed to the effect of tissue tension on the orientation of the interphase long axis (20–22).

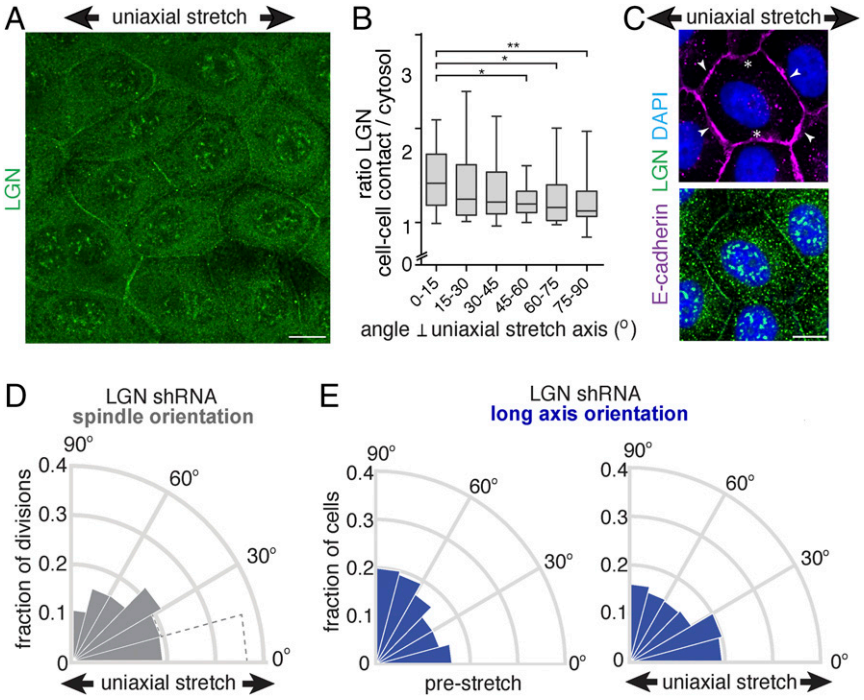

Fig. 5. Uniaxial stretch orients cell divisions through LGN. (*A*) Immunostaining of endogenous LGN in MDCK cells upon application (at least 1 h) of 12% uniaxial stretch, showing the polarized distribution of LGN, which becomes mostly enriched at cell–cell contacts perpendicular to the stretch axis and less at cell–cell contacts parallel to the stretch axis. (*B*) Quantification of the intensity of LGN at the cell–cell contact relative to the underlying cytosol, with respect to the angle of the cell–cell contact relative to the stretch axis (0° is perpendicular to the stretch axis), with mean and SD from three independent experiments ($n = 76$ cells). *$P < 0.007$; **$P < 0.0001$, using a Mann–Whitney U test. (*C*) Immunostaining of endogenous LGN and E-cadherin in MDCK cells upon application of (at least 1 h of) 12% uniaxial stretch, showing the polarization of LGN upon uniaxial stretch with enrichment at the cell cortex perpendicular to the stretch axis (arrowheads) and less at the cortex parallel to the stretch axis (white asterisks), whereas E-cadherin remains uniformly localized at the plasma membrane. (*D*) Circular frequency histograms (Rose diagrams) of the mitotic spindle angle relative to the direction (at least 1 h) of 12% stretch in MDCK cells expressing LGN shRNA ($n = 162$) from three independent experiments. The distribution of the mitotic spindle angle in stretched control cells (as shown in Fig. 3*F*) is indicated in dotted lines. (*E*) Circular frequency histograms (Rose diagrams) of the distribution of the long axis angle relative to the direction of stretch in MDCK cells expressing LGN shRNA, before and after application of (at least 1 h of) 12% stretch, from three independent experiments with at least 500 cells per experiment. (Scale bars, 10 μm.)

This conclusion was further supported by studies in which high (30%) uniaxial stretch of a suspended MDCK cell monolayer resulted in a strong correlation between the orientations of the long axis of cells and cell division (24). Here, we minimized the effect of stretch on inducing cell shape (long axis) orientation by applying a low level of uniaxial stretch to a MDCK epithelial cell monolayer adhered to an ECM substrate. Whereas 12% axial strain did not produce a strong effect on cell shape (Fig. 2*B*), it was sufficient to induce a strong bias in the orientation of cell divisions in the strain axis (Fig. 1*D*). Importantly, we found little or no correlation between the orientation of cell division and long axis of cells that aligned their division with stretch (Fig. 2*E* and Fig. S1*H*). Instead, the long axis orientation of cells that divided in the direction of applied stretch was randomly distributed, and we detected cells that divided along their short axis (Fig. 2*E* and Fig. S1*H*). These data indicate that tensile forces can dominate over cell shape in determining division orientation. In support of a cell shape-independent regulation of cell division orientation by uniaxial stretch, 12% axial strain in MDCK cells lacking E-cadherin adhesion or LGN expression did not influence the orientation of cell divisions, whereas it produced changes in cell shape comparable to wild-type MDCK cells (Fig. S2 *A* and *B*).

Our results provide insight into the mechanism that couples tension across the tissue to cell division orientation. We showed that alignment of cell division orientation with uniaxial stretch requires the mechanosensitive adhesion protein E-cadherin that mediates the tension-sensitive recruitment of LGN to cell–cell contacts: (*i*) Cell divisions in cells expressing the truncated E-cadherin mutant T151, which is not subjected to external forces, were randomly oriented in the presence of uniaxial stretch, even though there was still a stretch-induced change in the cell long axis similar to wild-type MDCK cells (Fig. 3). (*ii*) LGN was recruited to cell–cell contacts in the presence of intrinsic tensile forces or ectopically applied stretch (Fig. 4). (*iii*) Uniaxial stretch resulted in the polarized distribution of LGN, which became enriched at cell–cell contacts perpendicular to the stretch axis (Fig. 5 *A*–*C*). (*iv*) Knockdown of LGN expression resulted in the random orientation of cell divisions relative to the direction of uniaxial stretch (Fig. 5*D*). Whereas our data indicate that E-cadherin and LGN are essential to couple tissue tension to spindle orientation, our findings do not rule out the possibility that cell elongation, the position of tricellular junctions (45), or other mechanosensitive cellular structures such as retraction fibers (46), may contribute to tension-oriented divisions, in particular under conditions of high tension with large cell deformation (20–22, 24).

Previously, we demonstrated that LGN directly interacts with the cytosolic tail of E-cadherin, which localizes LGN to cell–cell contacts (8), and that this interaction orients planar epithelial cell divisions. Here, we showed that the recruitment of LGN to E-cadherin adhesions is tension sensitive, and consequently E-cadherin aligns planar cell divisions with the direction of tension across the monolayer. Moreover, uniaxial stretch induced the polarized distribution of myosin IIA (Fig. 3 *A*–*C*) and the polarized recruitment of LGN to E-cadherin–based cell–cell junctions (Fig. 5*A*), both of which are indicative of anisotropic cortical tension. The polarized junctional recruitment of LGN is not explained by a local increase in E-cadherin levels, because E-cadherin did not appear to have a polarized distribution at those cell–cell contacts upon uniaxial stretch (Figs. 2*A* and 5*C*). Further studies are required to identify how tensile forces that are sensed by E-cadherin regulate the recruitment of LGN to E-cadherin adhesions. Force-dependent conformational changes in the E-cadherin cytosolic tail are unlikely to be required for LGN binding, because the tetratricopeptide repeat (TPR) domain of LGN binds directly to the naturally unstructured E-cadherin cytosolic tail in solution, and thus in the absence of force (8). Instead, tensile forces on the E-cadherin complex may promote LGN binding by relieving an inhibitory signal that is present when the native E-cadherin complex is under a low level of tension. This putative inhibitory signal could be another protein or a post-translational modification that competes with LGN for E-cadherin binding. Alternatively, tensile forces might induce the indirect recruitment of LGN to E-cadherin adhesions through tension-sensitive recruitment of additional, intermediate LGN-interacting proteins that may associate with the E-cadherin complex [e.g., discs large (DLG) (47), Afadin (48), and ezrin, radixin, moesin (ERM) proteins (49)]. However, we did not observe a polarized distribution of any of these proteins in the presence or absence of uniaxial stretch, as we did for LGN (Fig. S6).

We observed that at increasing cell density the recruitment of LGN to cell–cell contacts decreased (Fig. 4*A*). This decrease could be restored by application of biaxial stretch to high-density monolayers (Fig. 4*B*), which suggests that the inverse correlation of junctional LGN levels with cell density may be a consequence of different levels of intercellular tension at different cell densities. It has been shown that as monolayer density increases, MDCK cells become less motile (39) and traction forces exerted on the substrate decrease (50). This implies that intercellular tension decreases with increasing cell density, as traction forces are balanced by intercellular stresses (51), and there is a direct relationship between the total cellular traction force on the ECM and cell–cell forces (52).

LGN orients cell divisions by localizing NuMA, which provides cortical anchorage sites for spindle astral microtubules and applies a pulling force on those microtubules through associated dynein (7). In line with our results indicating the requirement of LGN for tension-oriented divisions, keratinocytes do not align divisions with uniaxial stretch in the absence of NuMA (53). In contrast to LGN, NuMA is not present at cell–cell contacts during interphase in MDCK cells, but is restricted to the nucleus (6, 8). Upon nuclear envelope breakdown and mitotic entry, NuMA is released from the nucleus and competes LGN from E-cadherin to locally form the LGN/NuMA complex (8). The LGN/NuMA complex then stabilizes cortical associations of astral microtubules at cell–cell adhesions and orients the mitotic spindle. We observed a stretch-induced, polarized recruitment of LGN to cell–cell contacts in interphase cells before mitotic entry (Fig. 5). This polarized distribution of LGN defines the cortical distribution of NuMA upon mitotic entry (8), and, consistent with this function of LGN, we observed that both LGN and NuMA accumulated at the cortex of mitotic cells perpendicular to the direction of uniaxial stretch (Fig. S5 *C* and *D*). The tension-sensitive junctional localization of LGN before mitotic entry indicates that the recruitment of LGN to cell–cell contacts is uncoupled from putative mechanical changes due to mitotic rounding (54). Of note, NuMA may translate not only cell–cell junctional tension but also interphase cell shape to the orientation of the mitotic spindle, as shown for its *Drosophila* homolog Mud, albeit in an LGN-independent manner (45). However, it remains to be determined whether this mechanism exists in mammalian epithelia, as Mud lacks a nuclear localization motif and, in contrast to mammalian NuMA, is not restricted to the nucleus in interphase cells (6).

Taken together, we identified a key role of E-cadherin and LGN in transducing tension across a tissue monolayer to orient the mitotic spindle, which can establish tension-oriented cell division in the absence of cell shape changes. Cell division alignment with anisotropic tension may coordinate tissue expansion during morphogenesis and contribute to equalizing tension across a tissue, which can become highly anisotropic as a result of localized proliferation or morphogenetic events (55). Our findings thus support a prominent function of E-cadherin in the mechanical regulation of tissue morphogenesis.

Methods

Antibodies. The following commercial antibodies were used at the indicated concentrations: Afadin (Sigma, A0349; 1:200), α-tubulin (DM1A, Sigma; 1:1,000),

DECMA-1 (GeneTex, GTX11512; 1:500), DLG1 (2D11, Santa Cruz Technologies, H-60; 1:200), HA (Sigma, H6908; 1:250), LGN (Millipore, ABT-174; 1:250), NuMA (Abcam, ab36999; 1:250), pERM (phospho-Ezrin T567, phosho-Radixin T564, phospho-Moesin T558; Cell Signaling, 3141; 1:250), and rr1 (mouse; Developmental Studies Hybridoma Bank; 1:250).

Cell Culture. Parental MDCK GII cells, MDCK cells stably expressing E-cadherin-DsRed, GFP–α-tubulin, GFP-myosin IIA (a kind gift from So Yamada, University of California, Davis) (35) or truncated E-cadherin (T151) under control of a doxycycline-repressible promotor (38) were cultured at 37 °C and 5% CO_2 in low-glucose DMEM containing 10% FBS, 1 g/L sodium bicarbonate, and penicillin/streptomycin/kanamycin.

Cells were transfected using Lipofectamine 3000 (Life Technologies) according to the manufacturer's protocol. For lentiviral knockdown experiments, cells were infected with lentiviral shRNAs targeting LGN (TRCN0000011025, Mission shRNA plasmid, Sigma-Aldrich) or scrambled control (SHC002, Mission shRNA plasmid, Sigma-Aldrich) produced in HEK293T cells, and analyzed at least 3 d after infection.

Application of Uniaxial Stretch. MDCK cells were plated on a PDMS silicone-based cell stretching device with a 0.125-mm thick silicone membrane (Specialty Manufacturing), adapted from refs. 56, 57, with modifications for improved stretch repeatability and live-cell imaging (Fig. 1*A*). This stretching device was composed of a PDMS-based cell culture channel surrounded by pneumatic channels, which was fabricated through a molding process. For this process, PDMS elastomer and a curing agent (Sylgard 182, Dow Corning) were mixed at 10:1 wt/wt ratio and poured over a 3D-printed mold (Fused Deposition Modeling Dimension 1200es, Stratasys) and baked at 65 °C overnight. To smooth the surface peeled off from the 3D mold, the device was stamped on a thin layer of uncured PDMS, followed by baking at 65 °C for 3 h. Subsequently, the device was bonded with the silicone membrane using plasma activation of the surface (PDC-32G, Harrick Plasma). Following coating with rat tail collagen type I (Corning), a confluent density of MDCK cells (6×10^5 cells) was seeded in the central channel. One day following plating, cells were stretched using a pneumatic valve to control vacuum pressure in the two neighboring side channels. The strain field was evaluated by measuring the displacement of 2-μm diameter fluorescent beads (R0200, Thermo Fisher Scientific) and confirmed in cell experiments by measuring the displacement of nuclei in MDCK cell monolayers using custom MATLAB scripts to measure nearest neighbor distances (Mathworks). For immunostainings and spindle orientation measurements, cells were stretched for at least 1 h, and analyses were performed during application of stretch (either by live-cell imaging or by fixation of cells while under stretch) to avoid putative stress relaxation.

Analysis of the Orientation of the Cell Long Axis and Mitotic Spindle Orientation. All imaging of cell long axes and mitotic spindle orientations was performed with a customized Zeiss Observer inverted microscope (Intelligent Imaging Innovations, 3I) using a 20× objective (N.A. 0.75) in a temperature- and CO_2-controlled incubator. For cell shape determination, cell outlines were visualized by the localization of E-cadherin:DsRed. The long axis of cells (relative to the direction of applied stretch) before and after stretch was quantified in all individual cells within the monolayer using custom MATLAB scripts. The orientation of the mitotic spindle in late metaphase (the frame before anaphase onset) was determined by live-cell imaging of cells expressing GFP-tagged α-tubulin at 15-min intervals and measured using ImageJ software (NIH). In these cells, the plasma membrane was visualized with CellMask (Thermo), and the angle of the long axis in the frame before mitotic entry was measured using BioVoxxel in ImageJ.

We compared the mitotic spindle orientation relative to uniaxial stretch in wild-type, T151 E-cadherin, and LGN shRNA-expressing MDCK cells upon fixation in 4% paraformaldehyde (EM grade, Electron Microscopy Sciences), followed by permeabilization in 0.1% Triton X-100, and blocking in 1% BSA, 1% goat serum, 1% donkey serum. Cells were then incubated with the α-tubulin antibody and subsequently Alexa-labeled secondary antibody. Because in T151 E-cadherin and LGN shRNA-expressing MDCK cells the planar cell division is disrupted (20% and 21% of the cells divided perpendicular, respectively), only cells that divided within the epithelial plane were analyzed. The cell shape of these cells was visualized using live-cell imaging and plasma membrane visualization using CellMask (Thermo) and quantified in all individual cells within the monolayer using custom MATLAB scripts.

Analysis of Cortical Myosin Recruitment. To analyze the cortical distribution of myosin IIA, MDCK GFP-myosin IIA cells were plated on the uniaxial stretching device, and myosin IIA was visualized before and at least 1 h after the application of 12% uniaxial stretch using live-cell imaging. The presence of cortical GFP-myosin IIA was quantified and subsequently the distribution of the angles of GFP-myosin IIA relative to the stretch axis was quantified using ImageJ software and custom MATLAB scripts. A paired Student *t* test was used for statistical analysis.

LGN Immunostaining. Cells were fixed in ice-cold 100% methanol for 5 min, blocked in buffer containing 1% BSA, 1% goat serum, and 1% donkey serum, and incubated with the indicated antibodies and then Alexa-labeled secondary antibodies (Life Technologies) and Hoechst 33342 (Molecular Probes), and analyzed with a LSM 710 confocal microscope using a 63× objective (N.A. 1.4). When indicated, cells were pretreated for 5 min with 25 μM ML-7 (Sigma) or DMSO control before fixing. For quantification of cortical LGN in Fig. 4, the E-cadherin and Hoechst channels were used as masks, and the ratio of plasma membrane levels (in the E-cadherin mask) and cytosolic levels (excluded from the E-cadherin and nuclear mask) of LGN was measured using ImageJ software (NIH). A paired Student *t* test was used for statistical analysis. For quantification of junctional LGN polarization with uniaxial stretch in Fig. 5*B*, the ratio of LGN intensity at cell–cell contacts relative to the adjacent cytosol from both neighboring cells was quantified, as well as the angle of the cell–cell contact relative to the stretch axis, using ImageJ software (NIH). A Mann–Whitney *U* test was used for statistical analysis.

Application of Biaxial Stretch. MDCK cells were plated in wells containing a stretchable, collagen I-coated silicone membrane (0.254-mm thickness, Stockwell) in low-calcium (5 μM) DMEM with low glucose (200 mg/L). After 60 min, the medium was replaced by DMEM with normal calcium levels (1.8 mM). Stretch was applied 24 h after calcium switch for at least 1 h at 10% stretch using an integrated strain array, in which wells are placed over pillars in an acrylic pneumatic compartment (40). Vacuum pressure was applied using a microprocessor-based control system through the compartment to deform the silicone substrate around the pillar, resulting in biaxial stretching accompanied by equi-biaxial in-plane strain.

Functionalized Sidewalls. E-cadherin:Fc functionalized silicone sidewalls were fabricated as described (8, 41). In brief, scaffolds were constructed from 250-mm thick silicone sheeting (Bisco HT-6240, Stockwell Elastomers) cut into microwell inserts measuring 14 × 11 mm using a computer-controlled razor writer (Cameo, Silhouette), plasma activated using atmospheric plasma (50 W, 45 s, 500 mTorr, PDC-001, Harrick Plasma), silanized by immersion in a solution of 2% triethoxysilylundecanal (Gelest) and 2% triethylamine (Sigma) in pure ethanol (Goldshield), followed by baking at 85 °C for 3 h. A total of 250 mg/mL Protein A/G (Thermo-Pierce) in sodium cyanoborohydride coupling buffer (Sigma) was added to each well and allowed to react with the silanized stencils overnight at 4 °C. Stencils were washed with PBS-containing 0.1% Tween-20 (PBST), incubated for at least 1 h with 200 mg/mL E-cadherin:Fc at room temperature, and then with 10 mg/mL BSA for 30 min to neutralize remaining aldehydes and block exposed silicone. Functionalized stencils were transferred to tissue culture plastic imaging dishes (Ibidi-treat, Ibidi), and 2×10^3 MDCK cells were seeded in each well, which were tilted during plating to promote interactions of cells with the sidewalls. Cells were fixed and immunostained for LGN (as indicated above) at least 6 h following plating.

ACKNOWLEDGMENTS. We thank So Yamada (University of California, Davis) for MDCK GFP-myosin IIA cells, Marjolein J. Vliem [University Medical Center (UMC), Utrecht] for technical assistance, and Johan de Rooij (UMC, Utrecht) and members of our laboratories for helpful discussions. This work was supported by an NIH Training Grant T32GM007276 (to K.C.H.), a National Science Foundation (NSF) Graduate Research Fellowships Program (to J.T.), an NSF Emerging Frontiers in Research and Innovation grant (to W.J.N. and B.L.P.), a Stanford Bio-X research fellowship (to K.C.H., J.T., and J.Y.S.), a Stanford Bio-X grant (to W.J.N. and B.L.P.), the Ilju Foundation (J.Y.S.), Netherlands Organisation for Scientific Research Rubicon Fellowship 82511015 (to M.G.), Dutch Cancer Society (KWF) Fundamental Cancer Research Fellowship Buit 2012-5373 (to M.G.), and NIH Grant R35GM118064 (to W.J.N.).

1. Wang CC, Jamal L, Janes KA (2012) Normal morphogenesis of epithelial tissues and progression of epithelial tumors. *Wiley Interdiscip Rev Syst Biol Med* 4:51–78.
2. Ragkousi K, Gibson MC (2014) Cell division and the maintenance of epithelial order. *J Cell Biol* 207:181–188.
3. Macara IG, Guyer R, Richardson G, Huo Y, Ahmed SM (2014) Epithelial homeostasis. *Curr Biol* 24:R815–R825.
4. Williams SE, Fuchs E (2013) Oriented divisions, fate decisions. *Curr Opin Cell Biol* 25: 749–758.

5. Pease JC, Tirnauer JS (2011) Mitotic spindle misorientation in cancer: Out of alignment and into the fire. *J Cell Sci* 124:1007–1016.
6. Du Q, Macara IG (2004) Mammalian Pins is a conformational switch that links NuMA to heterotrimeric G proteins. *Cell* 119:503–516.
7. Gillies TE, Cabernard C (2011) Cell division orientation in animals. *Curr Biol* 21: R599–R609.
8. Gloerich M, Bianchini JM, Siemers KA, Cohen DJ, Nelson WJ (2017) Cell division orientation is coupled to cell-cell adhesion by the E-cadherin/LGN complex. *Nat Commun* 8:13996.
9. Takeichi M (2014) Dynamic contacts: Rearranging adherens junctions to drive epithelial remodelling. *Nat Rev Mol Cell Biol* 15:397–410.
10. Iskratsch T, Wolfenson H, Sheetz MP (2014) Appreciating force and shape—the rise of mechanotransduction in cell biology. *Nat Rev Mol Cell Biol* 15:825–833.
11. Siedlik MJ, Varner VD, Nelson CM (2016) Pushing, pulling, and squeezing our way to understanding mechanotransduction. *Methods* 94:4–12.
12. Fernandez-Sanchez M-E, Brunet T, Röper J-C, Farge E (2015) Mechanotransduction's impact on animal development, evolution, and tumorigenesis. *Annu Rev Cell Dev Biol* 31:373–397.
13. Heisenberg C-P, Bellaïche Y (2013) Forces in tissue morphogenesis and patterning. *Cell* 153:948–962.
14. Lecuit T, Yap AS (2015) E-cadherin junctions as active mechanical integrators in tissue dynamics. *Nat Cell Biol* 17:533–539.
15. le Duc Q, et al. (2010) Vinculin potentiates E-cadherin mechanosensing and is recruited to actin-anchored sites within adherens junctions in a myosin II-dependent manner. *J Cell Biol* 189:1107–1115.
16. Yonemura S, Wada Y, Watanabe T, Nagafuchi A, Shibata M (2010) alpha-Catenin as a tension transducer that induces adherens junction development. *Nat Cell Biol* 12: 533–542.
17. Yao M, et al. (2014) Force-dependent conformational switch of α-catenin controls vinculin binding. *Nat Commun* 5:4525.
18. Buckley CD, et al. (2014) Cell adhesion. The minimal cadherin-catenin complex binds to actin filaments under force. *Science* 346:1254211.
19. Mammoto A, Mammoto T, Ingber DE (2012) Mechanosensitive mechanisms in transcriptional regulation. *J Cell Sci* 125:3061–3073.
20. Campinho P, et al. (2013) Tension-oriented cell divisions limit anisotropic tissue tension in epithelial spreading during zebrafish epiboly. *Nat Cell Biol* 15:1405–1414.
21. Legoff L, Rouault H, Lecuit T (2013) A global pattern of mechanical stress polarizes cell divisions and cell shape in the growing Drosophila wing disc. *Development* 140: 4051–4059.
22. Mao Y, et al. (2013) Differential proliferation rates generate patterns of mechanical tension that orient tissue growth. *EMBO J* 32:2790–2803.
23. Minc N, Piel M (2012) Predicting division plane position and orientation. *Trends Cell Biol* 22:193–200.
24. Wyatt TP, et al. (2015) Emergence of homeostatic epithelial packing and stress dissipation through divisions oriented along the long cell axis. *Proc Natl Acad Sci USA* 112:5726–5731.
25. Huh D, et al. (2013) Microfabrication of human organs-on-chips. *Nat Protoc* 8: 2135–2157.
26. den Elzen N, Buttery CV, Maddugoda MP, Ren G, Yap AS (2009) Cadherin adhesion receptors orient the mitotic spindle during symmetric cell division in mammalian epithelia. *Mol Biol Cell* 20:3740–3750.
27. Inaba M, Yuan H, Salzmann V, Fuller MT, Yamashita YM (2010) E-cadherin is required for centrosome and spindle orientation in Drosophila male germline stem cells. *PLoS One* 5:e12473.
28. Le Borgne R, Bellaïche Y, Schweisguth F (2002) Drosophila E-cadherin regulates the orientation of asymmetric cell division in the sensory organ lineage. *Curr Biol* 12: 95–104.
29. Lu B, Roegiers F, Jan LY, Jan YN (2001) Adherens junctions inhibit asymmetric division in the Drosophila epithelium. *Nature* 409:522–525.
30. Yamashita YM, Jones DL, Fuller MT (2003) Orientation of asymmetric stem cell division by the APC tumor suppressor and centrosome. *Science* 301:1547–1550.
31. Borghi N, et al. (2012) E-cadherin is under constitutive actomyosin-generated tension that is increased at cell–cell contacts upon externally applied stretch. *Proc Natl Acad Sci USA* 109:12568–12573.
32. Thomas WA, et al. (2013) α-Catenin and vinculin cooperate to promote high E-cadherin-based adhesion strength. *J Biol Chem* 288:4957–4969.
33. Barry AK, et al. (2014) α-catenin cytomechanics: Role in cadherin-dependent adhesion and mechanotransduction. *J Cell Sci* 127:1779–1791.
34. Twiss F, et al. (2012) Vinculin-dependent Cadherin mechanosensing regulates efficient epithelial barrier formation. *Biol Open* 1:1128–1140.
35. Ueda S, Blee AM, Macway KG, Renner DJ, Yamada S (2015) Force dependent biotinylation of myosin IIA by α-catenin tagged with a promiscuous biotin ligase. *PLoS One* 10:e0122886.
36. Fernandez-Gonzalez R, Simoes SdeM, Röper JC, Eaton S, Zallen JA (2009) Myosin II dynamics are regulated by tension in intercalating cells. *Dev Cell* 17:736–743.
37. Pouille P-A, Ahmadi P, Brunet A-C, Farge E (2009) Mechanical signals trigger Myosin II redistribution and mesoderm invagination in Drosophila embryos. *Sci Signal* 2:ra16.
38. Troxell ML, et al. (2000) Inhibiting cadherin function by dominant mutant E-cadherin expression increases the extent of tight junction assembly. *J Cell Sci* 113:985–996.
39. Puliafito A, et al. (2012) Collective and single cell behavior in epithelial contact inhibition. *Proc Natl Acad Sci USA* 109:739–744.
40. Simmons CS, et al. (2011) Integrated strain array for cellular mechanobiology studies. *J Micromech Microeng* 21:54016–54025.
41. Cohen DJ, Gloerich M, Nelson WJ (2016) Epithelial self-healing is recapitulated by a 3D biomimetic E-cadherin junction. *Proc Natl Acad Sci USA* 113:14698–14703.
42. Cai D, et al. (2014) Mechanical feedback through E-cadherin promotes direction sensing during collective cell migration. *Cell* 157:1146–1159.
43. Ladoux B, et al. (2010) Strength dependence of cadherin-mediated adhesions. *Biophys J* 98:534–542.
44. Liu Z, et al. (2010) Mechanical tugging force regulates the size of cell–cell junctions. *Proc Natl Acad Sci USA* 107:9944–9949.
45. Bosveld F, et al. (2016) Epithelial tricellular junctions act as interphase cell shape sensors to orient mitosis. *Nature* 530:495–498.
46. Fink J, et al. (2011) External forces control mitotic spindle positioning. *Nat Cell Biol* 13: 771–778.
47. Bergstralh DT, Lovegrove HE, St Johnston D (2013) Discs large links spindle orientation to apical-basal polarity in Drosophila epithelia. *Curr Biol* 23:1707–1712.
48. Carminati M, et al. (2016) Concomitant binding of Afadin to LGN and F-actin directs planar spindle orientation. *Nat Struct Mol Biol* 23:155–163.
49. Machicoane M, et al. (2014) SLK-dependent activation of ERMs controls LGN-NuMA localization and spindle orientation. *J Cell Biol* 205:791–799.
50. Kocgozlu L, et al. (2016) Epithelial cell packing induces distinct modes of cell extrusions. *Curr Biol* 26:2942–2950.
51. Tambe DT, et al. (2011) Collective cell guidance by cooperative intercellular forces. *Nat Mater* 10:469–475.
52. Maruthamuthu V, Sabass B, Schwarz US, Gardel ML (2011) Cell-ECM traction force modulates endogenous tension at cell–cell contacts. *Proc Natl Acad Sci USA* 108: 4708–4713.
53. Seldin L, Poulson ND, Foote HP, Lechler T (2013) NuMA localization, stability, and function in spindle orientation involve 4.1 and Cdk1 interactions. *Mol Biol Cell* 24: 3651–3662.
54. Ramkumar N, Baum B (2016) Coupling changes in cell shape to chromosome segregation. *Nat Rev Mol Cell Biol* 17:511–521.
55. Nestor-Bergmann A, Goddard G, Woolner S (2014) Force and the spindle: Mechanical cues in mitotic spindle orientation. *Semin Cell Dev Biol* 34:133–139.
56. Huh D, et al. (2010) Reconstituting organ-level lung functions on a chip. *Science* 328: 1662–1668.
57. Zhao FH, Kreutzer J, Pajunen S, Kallio P (2014) Mechanical analysis of a pneumatically actuated concentric double-shell structure for cell stretching. *Micromachines (Basel)* 5: 868–885.